Research Article GU J Sci 38(1): 115-129 (2025) DOI: 10.35378/gujs.1475805

Gazi University

Journal of Science

http://dergipark.gov.tr/gujs

Fusion of Image Transformation Techniques for IoT-based Multivariate Time-Series

Imran BAMUS, Feyza YILDIRIM OKAY*, Abdullah Enes GUN, Sedef DEMIRCI

Gazi University, Computer Engineering Department, 06570, Ankara, Türkiye

Highlights

- Focuses on predicting complex patterns within a IoT multivariate time-series dataset.
- Proposes fusion of image transformation techniques in different orientations.
- CNN is employed to extract features of the fused images.
- The fused image transformation techniques outperform traditional image transformation techniques.

Article Info

Received: 30 Apr 2024
Accepted: 04 Oct 2024

Keywords

IoT
Time-series data
Image transformation
Fusion
Deep learning

Abstract

The emergence of the Internet of Things (IoT) has ushered in a new era of data generation with the opportunity for data to become a key element of connected devices. This study investigates new methods to bridge the realms of multivariate time-series data and image analysis, paying special attention to Gramian Angular Summation Field (GASF), Gramian Angular Difference Field (GADF), Markov Transition Field (MTF), and Recurrence Plot (RP) transformation techniques. These techniques serve to convert raw time-series data into visual representations, laying the foundation for deeper analysis and predictive modeling. The study introduces a novel paradigm by not only employing individual image transformation techniques but also fusing them in both horizontal and square orientations. By leveraging Convolutional Neural Networks (CNNs), this study demonstrates the efficiency of innovative fused-oriented image transformation techniques in predicting complex patterns within a multivariate time-series dataset related to electricity distribution and transformer oil temperature. The experimental results indicate that the Fused-Horizontal image transformation technique, using the order RP - GADF - MTF - GASF, yields the best performance, achieving the lowest MSE of 0.01047, RMSE of 0.10235, and MAE of 0.08054. Additionally, the order RP - GADF - GASF - MTF results in the lowest MAPE of 0.21997, outperforming both Fused-Square techniques and individual methods like GASF, GADF, MTF, and RP. These findings underscore the potential of fused image transformation techniques in improving prediction accuracy, offering a significant advancement over traditional methods.

1. INTRODUCTION

The rise of the Internet of Things (IoT) in recent years has transformed various industries by enabling the connection of devices and the generation of vast amounts of data. This interconnected network of devices, sensors, and systems allows for real-time monitoring, data collection, and decision-making, which are crucial for optimizing operations, improving efficiency, and preventing potential failures. A significant portion of the data generated by IoT devices is time-series data, which captures the progression of events over time, providing insights into patterns, trends, and anomalies that are vital for predictive modeling and decision-making processes [1].

Time-series IoT data plays a pivotal role in industries such as healthcare, agriculture, manufacturing, energy management, smart cities, finance and transportation, where it is used to monitor critical parameters, forecast future events, and detect anomalies that could indicate potential issues [2-5]. However, traditional analysis methods often struggle to reveal the complex patterns and correlations within this data, especially in multivariate contexts where multiple variables interact in complex ways [6].

*Corresponding author, e-mail: feyzaokay@gazi.edu.tr

In the existing literature, various image transformation techniques, such as Gramian Angular Summation Field (GASF), Gramian Angular Difference Field (GADF), Markov Transition Field (MTF), and Recurrence Plot (RP), have been explored as a means of converting time-series data into visual representations [7]. These visual representations allow for the application of advanced image processing and deep learning techniques, such as Convolutional Neural Networks (CNNs), to extract features and make predictions based on the transformed data. However, the focus has predominantly been on applying these techniques individually, which may limit their effectiveness in capturing the full complexity of multivariate time-series data.

The gap in the literature lies in the limited exploration of combining multiple image transformation techniques to enhance predictive accuracy. While some studies have attempted to fuse different image transformation methods, they often do so in a limited manner, without fully exploring the potential of different fusion orientations and orders. This study addresses this gap by proposing the fusion of GASF, GADF, MTF, and RP techniques in both horizontal and square orientations, experimenting with different fusion orders to create more comprehensive representations of the data. By leveraging CNNs to analyze these fused images, our approach introduces a novel and powerful dimension to predictive modeling in IoT multivariate time-series data. Our contribution is twofold: first, we demonstrate the superiority of fused image transformation techniques over individual methods in predicting complex patterns within time-series data; second, we provide a detailed comparison of different fusion orientations and orders, highlighting the best-performing configurations. This study not only fills the gap in the literature but also offers a practical approach for improving predictive accuracy in industries reliant on IoT and time-series data.

The remaining part of this paper is organized as follows: Section 2 highlights existing studies in the literature, providing a comprehensive overview. Section 3 details the theoretical background of the four primary image transformation techniques – GASF, GADF, MTF, and RP – clarifying their unique contributions. Section 4 introduces the dataset used in the study, offering a detailed description of its characteristics and significance. Section 5 outlines the proposed approach, emphasizing the fused orientation of image transformation techniques using CNNs. Section 6 presents experimental evaluation and discusses the experimental results to showcase the effectiveness of our approach. Lastly, Section 7 concludes the paper by summing up the key findings and suggesting avenues for future exploration.

2. LITERATURE REVIEW

The exploration of time-series data and image analysis within the IoT context has garnered attention in recent research endeavors. Image transformation techniques have become popular for uncovering hidden patterns in time-series data by transforming them into images. These techniques are commonly applied in various fields, including security, healthcare, industrial, environmental, smart homes, and finance domains [8-17]. This section offers an overview of existing studies, as depicted in Table 1, that contribute to the comprehension and manipulation of IoT data, with a focus on time-series data and image transformation techniques.

Baldini et al. [8] explored the use of RP image transformation and CNNs for IoT device authentication. This approach, known as radiometric identification, showed improved performance in device identification. The RP-CNN method, particularly with a threshold of 0.02, achieved an accuracy of 99.4%, outperforming other methods. Similarly, Ferraro et al. [9] proposed the use of GAF with a CNN model to improve predictive maintenance, conducting experiments on the BackBlaze dataset. They compare their results with those of an LSTM model presented in an existing study. According to their findings, the proposed data transformation techniques demonstrate superior performance in terms of accuracy, precision, and recall. The best results are achieved for both a prediction window of 45 days and a time window of 14 days. The work of Hammoud et al. [10] presented a deep learning framework for diagnosing neurological diseases using near-infrared eye video and time-series imaging algorithms. The methodology involves extracting pupil features from eye recordings and representing them as images through the GADF imaging method. These output images are then used to train a disease-detection model. Eye recordings from patients with Parkinson's disease (PD), Progressive Supranuclear Palsy (PSP), and Healthy Controls (HC) are included in the dataset. The optokinetic exercise produced the best classification results, with best accuracy for the

left, right, and both eyes. The study highlights how artificial intelligence might improve Internet of Medical Things (IoMT) applications for healthcare decision support.

In another paper, Wang and Kuo [11] tackled the challenge of detecting entanglement anomalies in dyeing machines, a critical quality bottleneck for small and medium-sized enterprises in Taiwan. They develop an innovative solution that combines GAF and MTF with CNN to create an entanglement detection model. The study is based on over 1.75 million pieces of production data collected in collaboration with industry manufacturers and universities. The model demonstrates remarkable effectiveness, as evidenced by the optimal detection time of 220 seconds for entanglement. Implementation of this system in the field leads to quick problem resolution, significantly reducing quality loss and downtime. Deng et al. [12] developed Wavelet Gramian CNN (WGCNN) to recognize non-line-of-sight signals in ultra-wideband indoor positioning systems. The model uses wavelet analysis for signal denoising and GAF for temporal correlation. Additionally, a GAF image reorganization strategy is performed to capture key sub-images, thereby eliminating the impact of invalid image sections. Finally, these reorganized sub-images are input into the CNN model to develop an LOS/NLOS classifier. The model is tested on the EU Horizon 2020 program dataset. Performance indicators show that the model achieved a higher recognition rate with an average accuracy increase of 3.09% over traditional CNN models. Furthermore, Lee et al. [13] proposed image transformation techniques for load prediction at the single household level. The authors employ GASF, GADF, MTF, and RP image transformation techniques alongside CNN and compare the results with Support Vector Machine (SVM), Artificial Neural Network (ANN), and one-dimensional CNN. The results indicate that RP with CNN yields superior prediction performance in terms of MAE, RMSE, and MAPE. Abidi et al. [14] proposed Encodeep, a fusion of four different image transformation techniques—GASF, GADF, RP, and MTF—integrated with a ResNet model for univariate and multivariate satellite image time series. They compare their results with fusion of two techniques (GASF and GADF), and fusion of three techniques (GASF, GADF, and MTF). The authors demonstrate that their proposed model achieves superior performance in terms of accuracy, F1-score, and Kappa score.

In the literature, image transformation techniques are more commonly used for classification problems. However, some studies propose them as solutions for prediction problems as well. Yang et al. [15] proposed a data transformation approach for multivariate time series using the Wafer dataset, which is employed to monitor semiconductor microelectronics manufacturing. They integrate GASF and GADF into a CNN model. The results are compared with several methods from the literature in terms of error rates, and superior results are obtained. Additionally, the authors investigate the impact of appending order by comparing p-values. The results indicate that appending order does not significantly influence error rates. Jiang et al. [16] performed four different image transformation techniques based on GSDF, GADF, MTF, and RP using three pre-trained CNN models, including VGG-11, ResNet-18, and DenseNet-121, on the M1 and M3 competition datasets. They also combined all techniques into a single fused image to achieve improved classification rates and forecasting error results compared to individual techniques. According to their findings, the proposed fused method outperforms the singular techniques across both evaluation metrics. Cheng et al. [17] proposed using GAF with an aggregated Residual Transform Neural Network (ResNext) to improve tool wear prediction and enhance machining quality. This technique transforms one-dimensional signals into two-dimensional data. The results are compared to results using 1D-CNN in terms of RMSE, MAE, and MAPE, demonstrating superior prediction performance.

While individual techniques have been studied, the fusion of multiple image transformation techniques remains relatively unexplored. Our approach builds upon the works of Jiang et al. [16]. In this study, the authors combined GAF, MTF and RP using fused-square orientation for improved representation of multivariate time-series data. However, our study integrates the same techniques and proposes two different orientations, including horizontal and square, and experiments with their different orders for enhanced predictive modeling.

Table 1. *Comparison of existing studies on image transformation techniques*

Study	**Year**	**Image Tran. Technique**	**Deep Learning Model**	**Application Domain**	**Problem Type**	**Key Findings**
Baldini et al. [8]	2018	RP	CNN	IoT device authentication	Authentication	RP-CNN achieved: Accuracy: 99.4% with a threshold of 0.02
Ferraro et al. [9]	2020	GAF	CNN	Predictive Maintenance	Classification	Higher classification results with GAF+CNN: Accuracy:96.25% Precision:96.13% Recall: 98.34%
Hammoud et al. [10]	2023	GADF	CNN	Neurological disease detection	Classification	The optokinetic exercise produced the best classification results with: Accuracy for the left: 96.9% Accuracy for right: 90.8% Accuracy of both eyes: 96.9%
Wang et al. [11]	2023	GAF MTF	CNN	Textile manufacturing	Detection	The best detection time for entanglement is: MTF: 220 seconds (reduced from 13.5 seconds with XGBoost)
Deng et al. [12]	2023	GAF	CNN	Smart home systems	Recognition	The average recognition accuracy of wavelength: GAF-CNN: 82.63% (3.09% higher than that of standard CNN.)
Lee et al. [13]	2023	MTF	CNN	Object location recognition	Recognition	MTF with artificial noise injection achieved: Accuracy: 97.43%
Abidi et al. [14]	2023	GASF GADF MTF RP Fused(Square)	ResNet-50	Monitoring	Classification	Higher results of Encodeep with: Accuracy: 90.22 F1-score: 90.26 Kappa: 85.86
Yang et al. [15]	2019	GASF GADF	CNN	Manufacturing	Prediction	Lower error rates: GASF: 1.06 GADF:1.57
Jiang et al. [16]	2022	GAF MTF RP Fused (Square)	ResNet-18, DenseNet-121, VGG-11	Micro-economic and industry	Prediction	Fused image forecasting error rates of MAPE with: ResNet-18: 11.89 DenseNet-121: 11.70 VGG-11: 11.67
Cheng et al. [17]	2024	GAF	ResNext	Manufacturing	Prediction	Higher prediction results: RMSE:6.96 MAE:5.44 MAPE:5.95
Our study	2024	GAF MTF RP Fused (Square, Horizontal)	CNN	Energy management	Prediction	Horizontally fused orientation performed best with: MSE: 0.01047 RMSE:0.10235 MAE:0.08054 MAPE:0.21997

3. PRELIMINARIES

This section presents the four techniques used in the study to create images from time-series data. Using polar coordinates rather than the more common Cartesian coordinates, the first imaging approach is called GAF. Gramian Angular Summation Field (GASF) and Gramian Angular Difference Field (GADF) are the two primary representation types used in the GAF technique. Providing different insights into the time-series data, GASF records the sum of angles, whereas GADF depicts the differences between angles in the polar coordinate system [18]. The second technique, called MTF, uses a time-series image to depict a region of a discretized time-series' transition probabilities. Time-series can be divided into boxes using a variety of strategies. The third and final technique, RP, is a graphical representation of a square matrix used in complex data analysis that visualizes the moments when the state of a given dynamic system repeats. The columns and rows of the matrix compare the states of the system at different times.

3.1. Gramian Angular Field (GAF) Transformation

GAF is designed to transform time-series data into images using a matrix based on polar coordinates, preserving precise temporal correlations [18]. Given a time-series $x = x_1, x_2, \ldots, x_n$ consisting of n real-valued observations, we normalize x so that all values fall within the interval [-1, 1] to obtain x, considering that the values of the time-series are scalar quantities rather than vectors

$$\tilde{x} = \frac{(x_i - \max(x)) + (x_i - \min(x))}{\max(x) - \min(x)} \tag{1}$$

where x_i represents an individual data point within the dataset, $max(x)$ and $min\,(x)$ represent the maximum and minimum value within the dataset. Then, the newly normalized values are represented within the polar coordinate system, where each point on the plane is defined by its distance from a reference point and its angle from a reference direction. This representation employs the angular cosine to encode the time stamp value as the radius

$$\begin{cases} \varphi = \arccos(\bar{x}_i), -1 \leq \bar{x}_i \leq 1, \bar{x}_i \in \bar{X} \\ r = \frac{t_i}{N}, t_i \in N \end{cases} \tag{2}$$

where ϕ denotes the angle, serving as a fixed parameter controlling the polar coordinate system. t_i represents the timestamp. N refers to the polar coordinate plane. r represents the radius. The function $arccos$ is the inverse cosine function applied to x, where $-1 \leq x_i \leq 1$.

Utilizing this data converted into a polar coordinate system, there are two distinct techniques to transform the normalized vectors into a symmetric matrix, considering both temporal and spatial. The GASF and GADF, utilize trigonometric addition in Equation (3) and subtraction and Equation (4), respectively [18].

- **Gramian Angular Summation Field (GASF):** Calculates the cosine of the angular addition of two points and shows the relationship between each point:

$$GASF(i,j) = \cos(\phi_i + \phi_j) \tag{3}$$
$$GASF = \tilde{X}'.\tilde{X} - \sqrt{I - \tilde{X}^2}'.\sqrt{I - \tilde{X}^2}.$$

- **Gramian Angular Difference Field (GADF):** Calculates the sine of the angular difference of two points and shows the relationship between each point:

$$GADF(i,j) = \sin(\phi_i - \phi_j) \tag{4}$$
$$GADF = \sqrt{I - \tilde{X}^2}'.\tilde{X} - \tilde{X}'.\sqrt{I - \tilde{X}^2}.$$

Figure 1 shows the time-series to image transformations steps in detail. In this figure, the raw time-series data is first scaled to the range $[-1,1]$ and converted into a polar coordinate systems. Then, it is transformed into the image by GASF and GADF techniques.

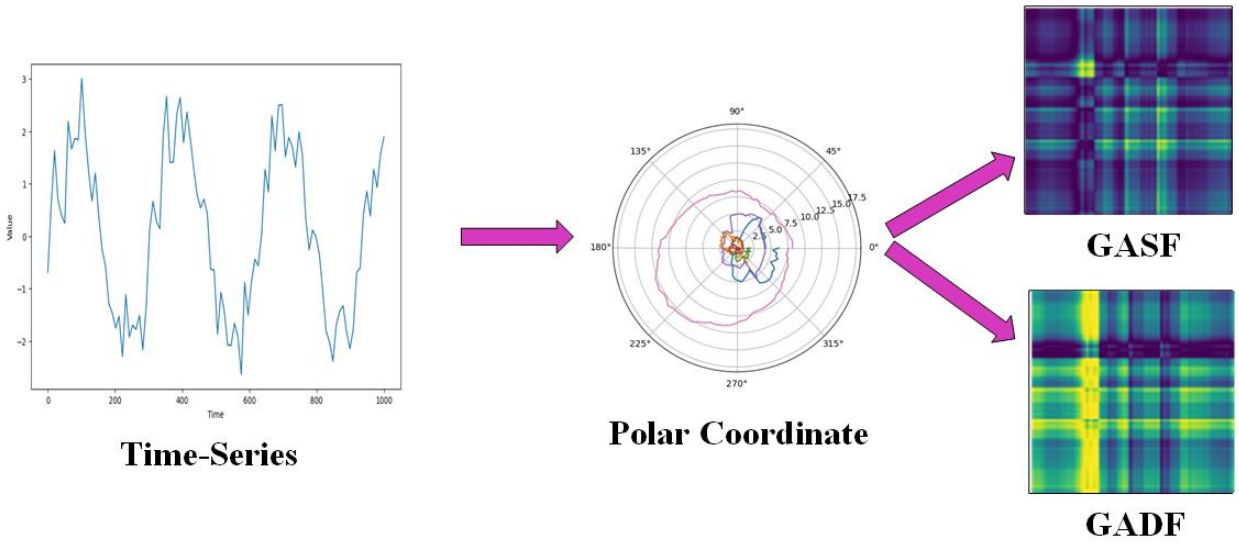

Figure 1. *The steps of time-series to image transformation using GAF technique (GASF, GADF)*

3.2. Markov Transition Field (MTF) Transformation

MTF relies on the probability transition matrix of a Markov chain obtained from the time-series analysis [19]. The normalized signal is divided into N non-overlapping sub-intervals. The Markov transition field (M) which is a matrix of size $Q \times Q$ is created from a given time-series and it is defined as the following matrix in Equation (5), showing the possibilities of transition from one state to another in the partitioned time-series:

$$M = \begin{bmatrix} w_{ij}|x_1 \epsilon q_i, x_1 \epsilon q_j & \cdots & w_{ij}|x_1 \epsilon q_i, x_N \epsilon q_j \\ w_{ij}|x_2 \epsilon q_i, x_1 \epsilon q_j & \cdots & w_{ij}|x_2 \epsilon q_i, x_N \epsilon q_j \\ \vdots & \ddots & \vdots \\ w_{ij}|x_N \epsilon q_i, x_1 \epsilon q_j & \cdots & w_{ij}|x_N \epsilon q_i, x_N \epsilon q_j \end{bmatrix}. \tag{5}$$

Figure 2 depicts the steps of raw time-series data to image transformation using MTF. The data is first transformed into Markov transition matrix and then MTF.

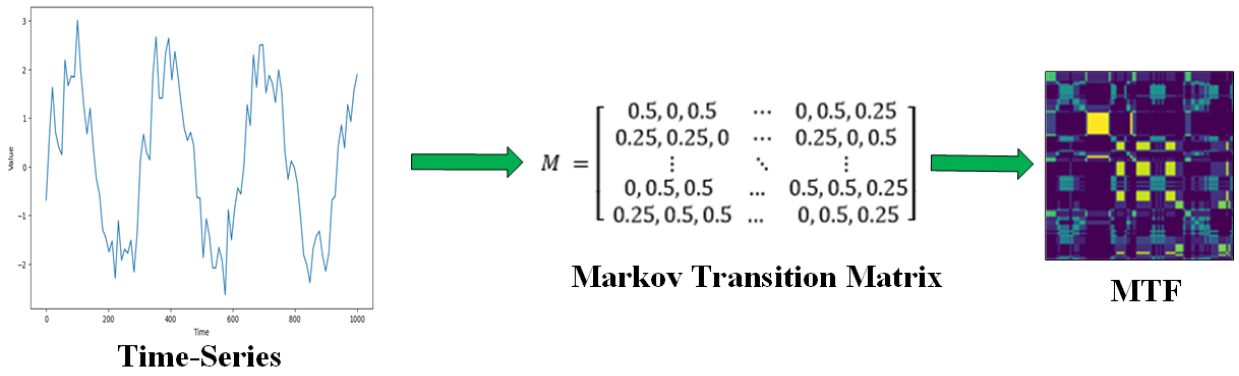

Figure 2. *The steps of time-series to image transformation using MTF technique*

3.3. Recurrence Plot (RP) Transformation

RP is constructed based on the recurrence of states in a phase space [20], outlined as follows

$$RP_{i,j}(\varepsilon) = \Theta(\varepsilon - ||X_i - X_j||) \,. \tag{6}$$

Here, ϵ represents a threshold distance that defines the radius within which states are deemed recurrent. $||X_i - X_j||$ denotes the distance between two states in the phase space. The Heaviside step function Θ returns a value of 1 if the distance is less than ϵ (indicating recurrence), and 0 otherwise. The resulting binary matrix RP visually represents the recurrent patterns present in the time-series data. Figure 3 indicates the graphical patterns reproduced for different sample times.

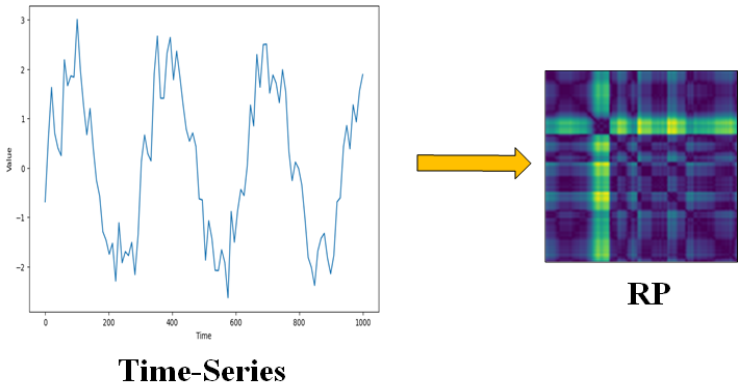

Figure 3. *The steps of time-series to image transformation using RP technique*

4. DATASET

The ETT-small-m1 dataset is used in the experiments [21]. Sequential utilization determines how energy is distributed among several regions in the distribution of power. However, it is challenging to predict a region's future demand. This dataset's goal is to predict when the electrical transformers' oil temperature will be safe and avoid unnecessary waste. Using this data, we are estimating the electric transformers' oil temperature and looking into their overload capacity.

The data is saved in.csv file format. Table 2 displays an example part of ETT-small-m1 data. There is a horizontal heading in the first line (8 columns) with the values "date", "HUFL", "HULL", "MUFL", "MULL", "LUFL", "LULL", and "OT." Table 3 provides a full explanation of each column name.

Table 2. *An example partial demonstration of ETT-small-m1 dataset*

	Date	HUFL	HULL	MUFL	MULL	LUFL	LULL	OT
0	2016-07-01 00:00:00	5.827	2.009	1.599	0.462	4.203	1.340	30.531000
1	2016-07-01 00:15:00	5.760	2.076	1.492	0.426	4.264	1.401	30.459999
2	2016-07-01 00:30:00	5.760	1.942	1.492	0.391	4.234	1.310	30.038000
3	2016-07-01 00:45:00	5.760	1.942	1.492	0.426	4.234	1.310	27.013000
4	2016-07-01 01:00:00	5.693	2.076	1.492	0.426	4.142	1.371	27.787001

Table 3. *Description of the abbreviations in the dataset*

Field	Date	HUFL	HULL	MUFL	MULL	LUFL	LULL	OT
Descriptions	The recorded date	High UseFul Load	High Use-Less Load	Middle UseFul Load	Middle UseLess Load	Low Use-Ful Load	Low Use-Less Load	Oil Temperature

5. PROPOSED MODEL: FUSION OF IMAGE TRANSFORMATION TECHNIQUES

This section explains the fused-oriented image transformation of time-series IoT data with the objective of demonstrating its superiority over individual image transformation techniques. As seen in Figure 4, the process of transformation and training consists of a total of three phases. The first phase involves acquiring 2D images using four different image transformation techniques of the original multivariate time-series data. The second phase involves combining images from four different types of transformation techniques. The third phase involves obtaining the results using a CNN model.

5.1. Image Transformation Phase

Image transformation converts multivariate IoT time-series data to 2D images using four transformation techniques. The main objective of this transformation is to reshape the attributes of the time data into image format, facilitating visual recognition and learning of underlying patterns. Four transformation techniques, namely GADF, GASF, MTF, and RP techniques, are employed to generate chronologically arranged 2D image sequences. After applying these techniques, four new types of images are generated: $X\_GADF, X\_GASF, X\_MTF, X\_RP$. We provide the entire time-series data as input to image transformation techniques by shifting it, resulting in an output of $Nx24x24$, indicating the completion of the transformation process. In the transformed images, colors closer to dark blue indicate smaller values, while colors closer to yellow represent values with greater amplitude, providing visual cues for the data's characteristics.

5.2. Image Fusion Phase

After completing the conversion process, X_{GADF}, X_{GASF}, X_{MTF}, X_{RP} are generated by employing GADF, GASF, MTF, and RP. These images represent NxN dimensional matrices, where X_{GADF}, X_{GASF}, X_{MTF}, X_{RP} are all R^{NxN}. These images can be further combined to create fused images, incorporating multiple perspectives of the time-series data. This fusion step involves two orientations: horizontal and square. The NxN images are fused with different orders of techniques to achieve $4xNxN$ for horizontal orientation and $2Nx2N$ for square orientation. This representation encapsulates valuable and comprehensive information, which can subsequently be assessed using image processing techniques.

5.3. Feature Extraction Phase via Convolutional Neural Network (CNN)

The fused images are trained utilizing CNN [22], a widely adopted deep learning algorithm. It is designed to process structured grid data, especially in the field of computer vision. CNNs capture spatial properties by applying a series of filters to the input data. Using multiple convolutional layers, they learn from simple patterns to complex high-level features. It usually includes convolutional layers, activation functions, pooling layers-larges, and fully connected layers. Each type of CNN contains specially designed convolution layers, activation functions, pooling layers and fully connected layers, tailored to the size and structure of the input data. Also, a sliding window approach is employed to enable prediction of the next location. This involves dividing the data into windows of a predetermined size and sequentially sliding them, enabling the prediction of the subsequent location. We set window size to 24. When converting the time-series data into a 2D image, we adapt each set of 24 rows within the window to be suitable for image transformation techniques in an $Nx24$ format depending on the number of columns (N).

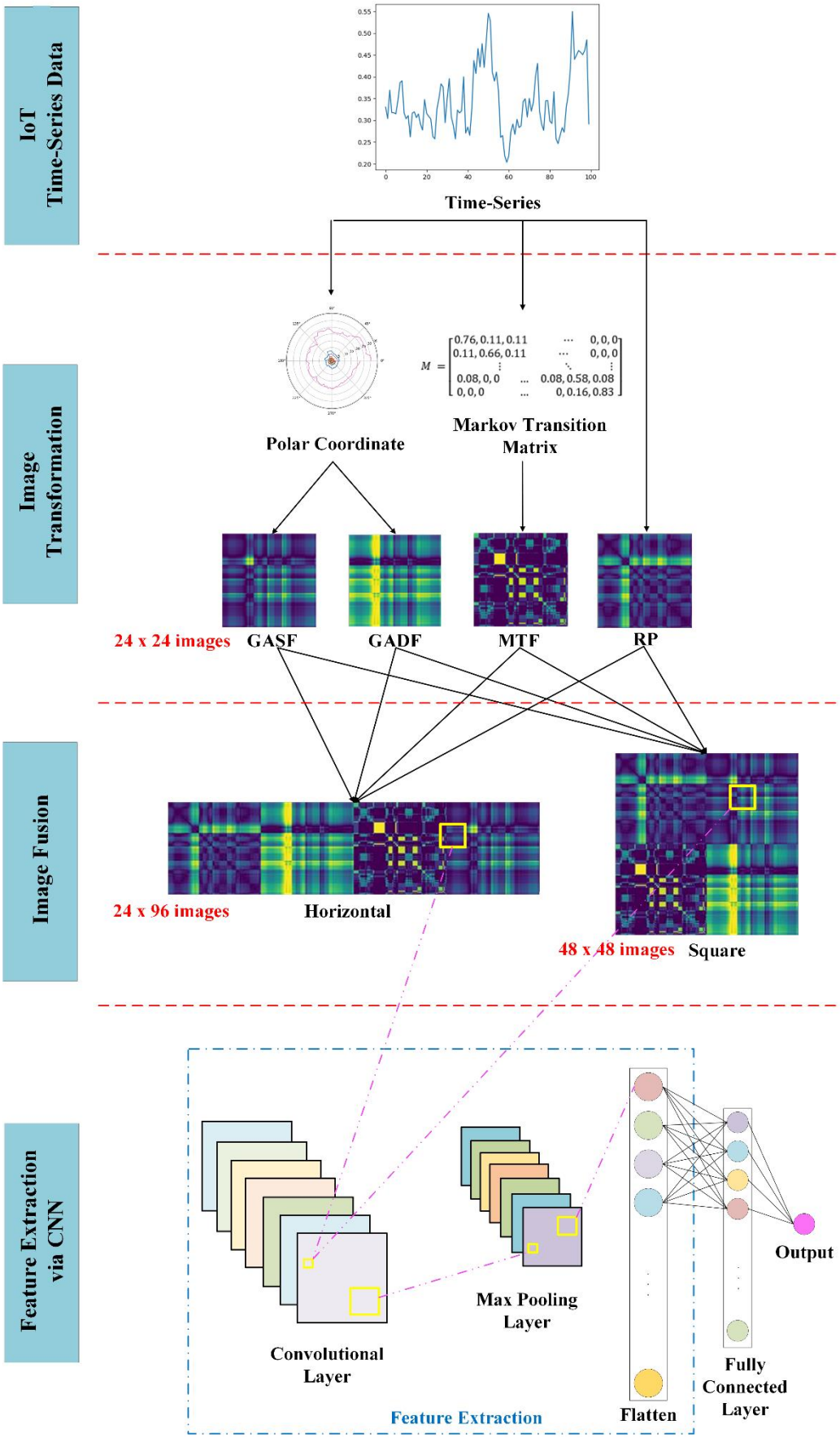

Figure 4. *The structure of proposed fused oriented image transformation techniques with CNN*

6. EXPERIMENTAL ANALYSIS

By presenting a combined approach, fused oriented image transformation approaches increase the effectiveness of image transformation techniques. This section compares the prediction outcomes of separate image transformation techniques such as GASF, GADF, MTF, and RP with the proposed fused oriented image transformation techniques with horizontal and square orientations. Performance evaluations are carried out based on the prediction success for each orientation in a comparative manner. Additionally, the results are compared with those obtained from individual image transformation techniques to underscore the success of the fused oriented image transformation techniques.

The methods in the experiments are implemented on VS Code. Also, several libraries are used with different purposes: PyTorch library to create the deep learning model, Pandas to manipulate our data in CSV format, Sclearn for scaler operations, Numpy to manipulate input arrays and results, and Matplotlib to visualize results. The Pyts library has been used to translate our data into images. CUDA is used in conjunction with Torch during model training and result acquisition.

6.1. Evaluation Metrics

We describe the evaluation metrics in this section that we used to evaluate the proposed model's performance. MSE, RMSE, and MAE are commonly used evaluation metrics in predictive models to measure the accuracy and performance of the model by quantifying the differences between predicted and actual values, shown in Equations (7)-(10) [23].

MSE measures the average of the frames of errors or residues. In the context of CNNs, this quantifies the difference between the estimated values (output of the neural network) and the actual target values (actual values)

$$MSE = \frac{1}{n}\sum_{i=1}^{n}(y_i - \bar{y_i})^2 \ . \tag{7}$$

RMSE is especially useful in situations where the unit of MSE cannot be directly exploited because the unit of RMSE is the unit of the target variable. Therefore, the RMSE provides a more interpretable value when measuring the difference between estimated values and actual target values

$$RMSE = \sqrt{\frac{1}{n}\sum_{i=1}^{n}(y_i - \bar{y_i})^2} \ . \tag{8}$$

MAE shows the average magnitude of the absolute difference between the estimated value and the actual value of each data point. MAE is more resilient than MSE, especially in the case of outliers in the dataset

$$MAE = \frac{1}{n}\sum_{i=1}^{n}|y_i - \bar{y_i}| \ . \tag{9}$$

MAPE shows the average size of the absolute percentage difference between the estimated value and the actual value of each data point. This measurement is especially useful for understanding how inaccurate the estimates are as a percentage relative to the original target variables

$$MAPE = \frac{100\%}{n}\sum_{i=1}^{n}\left|\frac{y_i - \bar{y_i}}{y_i}\right| \ . \tag{10}$$

6.2. Results and Discussion

In this study, images are generated using image transformation techniques including GASF, GADF, MTF, and RP applied to time-series data. Subsequently, these images are combined to generate fused images. In fused-oriented image transformation techniques, each image transformation technique, including GASF, GADF, MTF, and RP, is combined with different orientations, such as square or horizontal. Obtained image

datasets are partitioned into 80% for training and 20% for testing. Additionally, CNN is utilized to train both individual and fused images. Performance evaluation is conducted on an electricity transformer dataset by comparing both individual and fused versions, with different fusion orders. The results are analyzed based on various prediction evaluation metrics, including MSE, RMSE, MAE, and MAPE scores.

The hyperparameters of CNN for the proposed model are given in Table 4. Accordingly, 20 epochs are determined for the training phase. Adam optimizer is selected due to its faster calculation time and lower parameter requirements compared to others. Also, ReLU is determined as the activation function since it reduces the probability of encountering gradient vanishing problems. We use a sliding window approach for the prediction of the next time-series value. By splitting the data into windows of a specific size and sliding them one by one, the next value is predicted. In our proposed model, the sliding window size is set to 24.

Table 4. *Hyperparameters of CNN*

Parameters	**Values**
Input Size	24x24, 48x48, 24x96 (H x W)
Sliding Window Size	24
Number of Epochs	20
Pooling Function	Max Pooling (2x2)
Optimizer	Adam
Loss Function	MSE Loss
Activation Function	ReLU
Number of Units	17376

The fused-oriented image transformation techniques have stronger prediction capabilities compared to individual image transformation techniques. The prediction results vary according to the orientations and orders of these techniques. Tables 5 and 6 show prediction results for fused-oriented image transformation techniques with different orders. Specifically, Tables 5 and 6 indicate the MSE, RMSE, MAE, and MAPE results for horizontal and square orientations, respectively. The prediction scores change according to the orientations and fusion orders of individual techniques.

Table 5. *Different horizontal fusion orientations of image transformation techniques*

Fusion Order (horizontal)	**MSE**	**RMSE**	**MAE**	**MAPE**
RP - GADF - MTF - GASF	**0.01047**	**0.10235**	**0.08054**	0.23675
GADF - RP - GASF - MTF	0.01082	0.10404	0.08254	0.23685
RP - MTF - GADF - GASF	0.01159	0.10770	0.08539	0.24090
MTF - GADF - RP - GASF	0.01208	0.10994	0.08767	0.24625
RP - GADF - GASF - MTF	0.01220	0.11046	0.08743	**0.21997**
RP - MTF - GASF - GADF	0.01263	0.11239	0.08871	0.24664
MTF - GASF - RP - GADF	0.01263	0.11240	0.08991	0.26514
GADF - RP - MTF - GASF	0.01268	0.11264	0.09034	0.25425
GASF - MTF - GADF - RP	0.01328	0.11526	0.09185	0.27425
GASF - GADF - RP - MTF	0.01341	0.11581	0.09181	0.27118
MTF - GASF - GADF - RP	0.01361	0.11669	0.09164	0.26425
RP - GASF - GADF - MTF	0.01365	0.11684	0.09384	0.26454
RP - GASF - MTF - GADF	0.01371	0.11711	0.09249	0.27753
GASF - GADF - MTF - RP	0.01380	0.11747	0.09253	0.26988
GASF - RP - MTF - GADF	0.01387	0.11780	0.09448	0.27861
GASF - RP - GADF - MTF	0.01413	0.11889	0.09487	0.26403
GADF - GASF - MTF - RP	0.01421	0.11923	0.09396	0.27361
GADF - MTF - RP - GASF	0.01463	0.12096	0.09650	0.27025
GADF - GASF - RP - MTF	0.01521	0.12336	0.09671	0.28487

MTF - RP - GADF - GASF	0.01548	0.12443	0.09851	0.27097
GADF - MTF - GASF - RP	0.01604	0.12665	0.09963	0.30877
MTF - GADF - GASF - RP	0.01617	0.12719	0.09871	0.29808
MTF - RP - GASF - GADF	0.01689	0.12996	0.10066	0.29574
GASF - MTF - RP - GADF	0.01779	0.13339	0.10746	0.29392

When compared to different orders of fused oriented image transformation techniques, Table 5 shows that RP - GADF - MTF - GASF horizontal sequence has the highest prediction capability under all evaluation metrics, with the lowest MSE of 0.01047, RMSE of 0.10235, MAE of 0.08054. Also, RP - GADF - GASF - MTF horizontal sequence has the lowest MAPE of 0.21997. On the other hand, Table 6 shows that the RP - GASF - MTF - GADF square sequence exhibits the highest prediction capability, with the lowest MSE of 0.01153, RMSE of 0.10739, MAE of 0.08508. Also, GASF - MTF - RP – GADF square sequence has the lowest MAPE of 0.22757.

Table 6. *Different square fusion orientations of image transformation techniques*

Fusion Order (square)	**MSE**	**RMSE**	**MAE**	**MAPE**
RP - GASF - MTF - GADF	**0.01153**	**0.10739**	**0.08508**	0.25059
GADF - RP - MTF - GASF	0.01178	0.10853	0.08597	0.24990
GASF - MTF - GADF - RP	0.01195	0.10933	0.08673	0.25404
GASF - MTF - RP - GADF	0.01198	0.10948	0.08585	**0.22757**
RP - MTF - GASF - GADF	0.01209	0.10995	0.08671	0.25514
GADF - MTF - RP - GASF	0.01213	0.11017	0.08786	0.25728
RP - GADF - MTF - GASF	0.01247	0.11170	0.08952	0.25438
RP - GADF - GASF - MTF	0.01252	0.11191	0.08970	0.24968
MTF - GASF - RP - GADF	0.01256	0.11211	0.08962	0.25448
MTF - RP - GADF - GASF	0.01315	0.11467	0.08973	0.26424
GADF - GASF - MTF - RP	0.01319	0.11486	0.09096	0.27288
MTF - RP - GASF - GADF	0.01340	0.11577	0.09270	0.26976
MTF - GADF - RP - GASF	0.01391	0.11796	0.09189	0.28174
GASF - GADF - RP - MTF	0.01410	0.11877	0.09518	0.28260
MTF - GADF - GASF - RP	0.01437	0.11991	0.09664	0.27823
RP - GASF - GADF - MTF	0.01448	0.12033	0.09629	0.27632
GASF - RP - GADF - MTF	0.01449	0.12038	0.09462	0.29571
RP - MTF - GADF - GASF	0.01466	0.12109	0.09718	0.28891
MTF - GASF - GADF - RP	0.01467	0.12113	0.09649	0.27793
GASF - GADF - MTF - RP	0.01472	0.12135	0.09564	0.29089
GADF - MTF - GASF - RP	0.01517	0.12318	0.09892	0.27378
GADF - RP - GASF - MTF	0.01599	0.12648	0.10025	0.30083
GADF - GASF - RP - MTF	0.01629	0.12763	0.10259	0.29799
GASF - RP - MTF - GADF	0.01861	0.13643	0.10893	0.32141

Table 7 gives the comparative prediction results for fused oriented and individual techniques. According to the results, Fused-Horizontal image transformation techniques show superiority among Fused-Square oriented and individual techniques in terms of MSE, RMSE, MAE, and MAPE scores. Moreover, Fused-Square image transformation techniques have slightly lower prediction success with higher MSE, RMSE, MAE and MAPE scores than the Fused-Horizontal oriented techniques, but they still outperform GASF, GADF, MTF, and RP individual techniques. This suggests that combining multiple techniques through fusion enhances the predictive capacity and overall performance of the model. Among individual techniques, the RP technique has the best performance with the lowest prediction values, while MTF has the worst performance with the highest values.

Table 7. *Overall performance comparisons of fused and individual image transformation techniques*

Fused / Individual Image Transformation Techniques	**MSE**	**RMSE**	**MAE**	**MAPE**
Fused-Horizontal	0.01047	0.10235	0.08054	0.21997
Fused-Square	0.01153	0.10739	0.08508	0.22757
GASF	0.01705	0.13058	0.10306	0.31601
GADF	0.01573	0.12544	0.09876	0.29428
MTF	0.01973	0.14047	0.11050	0.34201
RP	0.01232	0.10928	0.08882	0.26374

In the existing literature [8-16], RMSE, MAE, and MAPE scores range from (i) 0.696 to 0.1833, (ii) 0.544 to 0.1505, and (iii) 0.595 to 0.2134, respectively. Although it would not be fair to compare our results with the results of these studies directly due to the use of different datasets, it is seen that the best RMSE and MAPE scores obtained in this study are reasonably high and in acceptable range. Additionally, it is seen that our study outperforms existing studies in terms of MAE score by achieving 0.08054.

7. CONCLUSION

This study has demonstrated the potential of fusing image transformation techniques to enhance the predictive power of deep learning algorithms for multivariate time-series data. The fusion of GAF, MTF, and RP techniques in both horizontal and square orientations, coupled with the use of CNN, has shown promising results in predicting complex patterns within a dataset related to electricity distribution and transformer oil temperature. The findings of this study have significant implications for the fields of IoT, multivariate time-series data analysis, image transformation, image fusion, and predictive modeling. This study provides a stepping stone towards the development of more sophisticated models for handling complex time-series data, paving the way for future advancements in this field. The experimental results demonstrate that the Fused-Horizontal image transformation technique with the order of RP - GADF - MTF – GASF exhibits the best performance, with the lowest MSE of 0.01047, RMSE of 0.10235, MAE of 0.08054. Also, the order of RP - GADF - GASF – MTF has the lowest MAPE of 0.21997, compared to both the Fused-Square image transformation techniques and other individual image transformation techniques such as GASF, GADF, MTF, and RP. Fused-Square image transformation techniques, on the other hand, show better performance than individual image transformation techniques. As a result, fused oriented image transformation techniques accelerate the performance of the image transformation techniques to reveal the hidden patterns in the time-series data. However, this study has certain limitations that should be acknowledged. First, the experiments were conducted using a single dataset, which may limit the generalizability of the findings to other types of IoT data or different domains. Additionally, the study focused on specific fusion techniques and CNN architectures, and other combinations or more advanced deep learning models could potentially yield different results. Furthermore, while the fusion techniques improved predictive performance, the computational complexity and processing time also increased, which could be a limiting factor in real-time or resource-constrained environments.

For future research, we plan to explore the performance of other image transformation techniques with different models of deep learning, including traditional machine learning models. Additionally, comparing the performance of applying the proposed approach to both univariate and multivariate time-series data could offer further insights and strengthen the generalizability of the findings. This study has opened up new avenues for leveraging advanced image transformation and fusion techniques to employ the power of time-series data for predictive modeling.

CONFLICTS OF INTEREST

No conflict of interest was declared by the authors.

REFERENCES

[1] Hu, C., Sun, Z., Li, C., Zhang, Y., and Xing, C., "Survey of Time-series Data Generation in IoT", Sensors, 23(15): 6976–6976, (2023).

[2] Kashani, M. H., Madanipour, M., Nikravan, M., Asghari, P., and Mahdipour, E., "A systematic review of IoT in healthcare: Applications, techniques, and trends", Journal of Network and Computer Applications, 192: 1-41, (2021).

[3] Bedi, G., Venayagamoorthy, G. K., Singh, R., Brooks, R. R., and Wang, K. C., "Review of Internet of Things (IoT) in electric power and energy systems", IEEE Internet of Things Journal, 5(2): 847-870, (2018).

[4] Oguz, F. E., Ekersular, M. N., Sunnetci, K. M., and Alkan, A., "Enabling Smart Agriculture: An IoT-Based Framework for Real-Time Monitoring and Analysis of Agricultural Data", Agricultural Research, 13: 574-585, (2024).

[5] Khanna, A., Kaur, S., "Internet of things (IoT), applications and challenges: a comprehensive review", Wireless Personal Communications, 114: 1687-1762, (2020).

[6] Estebsari, A., Rajabi, R., "Single residential load forecasting using deep learning and image encoding techniques", Electronics, 9: 1-17, (2020).

[7] Ye, X., Huang, Y., Bai, Z., and Wang, Y., "A novel approach for sports injury risk prediction: based on time-series image encoding and deep learning", Frontiers in Physiology, 14: 1-14, (2023).

[8] Baldini, G., Giuliani, R., and Dimc, F., "Physical layer authentication of Internet of Things wireless devices using Convolutional Neural Networks and Recurrence Plots", Internet Technology Letters, 2: 1-6, (2018).

[9] Ferraro, A., Galli, A., Moscato, V., and Sperlí, G., "A novel approach for predictive maintenance combining GAF encoding strategies and deep networks", In 2020 IEEE 6th International Conference on Dependability in Sensor, Cloud and Big Data Systems and Application (DependSys), IEEE, (2020).

[10] Hammoud, M., Kovalenko, E., Somov, A., Bril, E., and Baldycheva, A., "Deep learning framework for neurological diseases diagnosis through near-infrared eye video and time-series imaging algorithms", Internet of Things, 24: 1-20, (2023).

[11] Wang, C.-C., Kuo, C.-H., "Detecting dyeing machine entanglement anomalies by using time-series image analysis and deep learning techniques for dyeing-finishing process", Advanced Engineering Informatics, 55: 1-10, (2023).

[12] Deng, X., Ping, Z., and Sun, R., "UWB NLOS Recognition Based on Improved Convolutional Neural Network Assisted by Wavelet Analysis and Gramian Angular Field", IEEE Sensors Journal, 23(14): 16384-16392, (2023).

[13] Lee, H., Lee, J., "Convolutional Model with a Time-series Feature Based on RSSI Analysis with the Markov Transition Field for Enhancement of Location Recognition", Sensors, 23(7): 1-16, (2023).

[14] Abidi, A., Ienco, D., Abbes, A. B., and Farah, I. R., "Combining 2D encoding and convolutional neural network to enhance land cover mapping from Satellite Image Time-series", Engineering Applications of Artificial Intelligence, 122: 1-17, (2023).

[15] Yang, C. L., Yang, C. Y., Chen, Z. X., and Lo, N. W., "Multivariate time series data transformation for convolutional neural network", In 2019 IEEE/SICE International Symposium on System Integration (SII), IEEE, (2019).

[16] Jiang, W., Zhang, D. Ling, L., and Lin, R., "Time-series Classification Based on Image Transformation Using Feature Fusion Strategy", Neural Processing Letters, 54: 1-22, (2022).

[17] Cheng, Y., Lu, M., Gai, X., Guan, R., Zhou, S., and Xue, J., "Research on multi-signal milling tool wear prediction method based on GAF-ResNext", Robotics and Computer-Integrated Manufacturing, 85: 1-15, (2024).

[18] Mitiche, I., Morison, G., Nesbitt, A., Hughes-Narborough, M., Stewart, B., and Boreham, P., "Imaging Time-series for the Classification of EMI Discharge Sources", Sensors, 18(9): 1-17, (2018).

[19] Yan, J., Kan, J., and Luo, H., "Rolling Bearing Fault Diagnosis Based on Markov Transition Field and Residual Network", Sensors, 22(10): 3936–3936, (2022).

[20] Chen, Y., Su, S., and Yang, H., "Convolutional Neural Network Analysis of Recurrence Plots for Anomaly Detection", International Journal of Bifurcation and Chaos, 30(1): 201-213, (2020).

[21] "ETDataset/ETT-small at main · zhouhaoyi/ETDataset," GitHub. https://github.com/zhouhaoyi/ETDataset/tree/main/ETT-small. Accessed Date: 02 March 2024

[22] Jiang, J. R., Yen, and C. T., "Product quality prediction for wire electrical discharge machining with markov transition fields and convolutional long short-term memory neural networks", Applied Sciences, 11(13): 1-13, (2021).

[23] Plevris, V., Solorzano, G., Bakas, N., and Seghier, M. B., "Investigation of performance metrics in regression analysis and machine learning-based prediction models", 8th European Congress on Computational Methods in Applied Sciences and Engineering, (2022).